the plant journal

SEB SOCIETY FOR EXPERIMENTAL BIOLOGY

The Plant Journal (2022) **111,** 1324–1339 doi: 10.1111/tpj.15891

The ubiquitin–26S proteasome system and autophagy relay proteome homeostasis regulation during silique development

Peifeng Yu[1,2] **and Zhihua Hua**[1,2,*]

[1]*Department of Environmental and Plant Biology, Ohio University, Athens, Ohio 45701, USA, and*
[2]*Interdisciplinary Program in Molecular and Cellular Biology, Ohio University, Athens, Ohio 45701, USA*

Received 29 November 2021; revised 20 June 2022; accepted 28 June 2022; published online 3 July 2022.
*For correspondence (e-mail hua@ohio.edu).

SUMMARY

Functional studies of the ubiquitin–26S proteasome system (UPS) have demonstrated that virtually all aspects of the plant's life involve UPS-mediated turnover of abnormal or short-lived proteins. However, the role of the UPS during development, including in seeds and fruits, remains to be determined in detail, although mutants of several of its core elements are known to be embryonically lethal. Unfortunately, early termination of embryogenesis limits the possibility to characterize the activities of the UPS in reproductive organs. Given both the economic and the societal impact of reproductive production, such studies are indispensable. Here, we systematically compared expression of multiple 26S proteasome subunits along with the dynamics of proteasome activity and total protein ubiquitylation in seedlings, developing siliques, and embryos of *Arabidopsis thaliana*. Since autophagy plays the second largest role in maintaining proteome stability, we parallelly studied three rate-limiting enzymes that are involved in autophagy flux. Our experiments unexpectedly discovered that, in contrast to the activities in seedlings, both protein and transcript levels of six selected 26S proteasome subunits gradually decline in immature siliques or embryos toward maturation while the autophagy flux rises despite the nutrient-rich condition. We also discovered a reciprocal turnover pathway between the proteasome and autophagy. While the autophagy flux is suppressed in seedlings by UPS-mediated degradation of its three key enzymes, transcriptional reprogramming dampens this process in siliques, which in turn stimulates a bulk autophagic degradation of proteasomes. Collectively, our study of the developmental changes of the UPS and autophagy activities suggests that they relay the proteome homeostasis regulation in early silique and/or seed development, highlighting their interactions during development.

Keywords: development, 26S proteasome, autophagy, ubiquitylation, cellular homeostasis, protein degradation.

INTRODUCTION

Proteome homeostasis (proteostasis) is essential for maintaining life processes through regulating numerous metabolic pathways and providing structural materials. However, fluctuating internal and external environments often disrupt such stability, which indicates the regulatory machineries of proteostasis are an essential component of life. The ubiquitin (Ub)–26S proteasome system (UPS) and autophagy are two indispensable intracellular machineries that are responsible for removing and/or switching outdated metabolic pathways in all eukaryotic cells upon various internal and external cues (Pohl & Dikic, 2019). Yet how these two systems work in concert remains a big question in cellular quality control (Clavel & Dagdas, 2021; Ding et al., 2018; Minina et al., 2017).

In plants, the UPS is composed of many members, which can be temporarily and spatially separated into two subsystems that function in tandem for protein ubiquitylation and degradation. Protein ubiquitylation is a biochemical cascade reaction sequentially involving Ub-activating (E1), Ub-conjugating (E2), and Ub-ligating (E3) enzymes. Through ubiquitylation, a substrate is covalently modified by mono-Ub moieties or, in many cases, poly-Ub chains via the ε-amino group of its lysine (K) residues. If the substrate is modified by K48- or K11-linked poly-Ub chains, it will be recognized by the 26S proteasome for degradation

(Doroodian & Hua, 2021; Hellmann & Estelle, 2002; Hua & Vierstra, 2011; Marshall & Vierstra, 2019; Vierstra, 2009). While only a small proportion of the large ubiquitylation subsystem has been biochemically and functionally explored, the 26S proteasome has been relatively well dissected through proteomic, structural, and functional studies in yeast and Arabidopsis (see reviews by Finley et al., 2016; Finley & Prado, 2020; Marshall & Vierstra, 2019; Sahu & Glickman, 2021). It is composed of a hollow-shaped 20S catalytic core protease (CP) complex capped with one or two 19S regulatory particles (RPs) at its opposite ends (Beck et al., 2012; da Fonseca et al., 2012; Lander et al., 2012; Lasker et al., 2012). The RP unit can be further divided into two subcomplexes, lid and base, each with multiple subunits (Glickman et al., 1998). Among the RP subunits, Regulatory Particle Non-ATPase 1 (RPN1), RPN10, and RPN13 are important receptors for binding to poly-Ub chains that are conjugated with the ubiquitylation substrates (Martinez-Fonts et al., 2020). Upon the association with RP subunits, Ub moieties are cleaved by deubiquitylating enzymes (DUB), such as RPN11 and multiple loosely associated DUBs (Finley, 2009; Marshall & Vierstra, 2019), and released for reuse, while the substrate itself is unfolded and threaded into the CP compartment driven by Regulatory Particle Triple-A ATPase 1–6 (RPT1–6), which comprise the base of RP (Finley, 2009; Glickman et al., 1998; Smalle & Vierstra, 2004). The CP is composed of two outer hetero-heptameric α-rings and two inner hetero-heptameric β-rings assembling a hollow barrel-shaped chamber. Within this chamber, β-ring subunits possess three distinct types of proteases that harbor chymotrypsin-like, trypsin-like, and peptidyl-glutamyl peptide-hydrolyzing activities responsible for substrate degradation (Groll et al., 1997; Heinemeyer et al., 1997).

Autophagy is upregulated and serves as an alternative degradation machinery when eukaryotes experience nutrient stress conditions (see reviews by [Dikic & Elazar, 2018, Li & Vierstra, 2012, Marshall & Vierstra, 2018, Signorelli et al., 2019]). Through an expansion and enclosure process of a cup-shaped phagophore structure, a high volume of cytoplasmic contents, often including protein complexes/aggregates or even damaged organelles, can be engulfed to form double-membrane-enclosed autophagosomes (Soto-Burgos et al., 2018; Xie & Klionsky, 2007). Like many UPS substrates destined for turnover, the cargo carried in the internal vesicle of autophagosomes is eventually degraded into monomers for reuse by a group of hydrolases hosted in vacuoles (plants and fungi) or lysosomes (animals) who take them up through membrane fusion (Li & Vierstra, 2012; Marshall & Vierstra, 2018). While in many cases autophagy-mediated degradation occurs in bulk, recent studies have uncovered selective processes whose specificities are primarily determined by AuTophaGy-related 8 (ATG8) receptors (Marshall et al., 2019).

ATG8, a small Ub-like protein, is conjugated to the lipid phosphatidylethanolamine (PE) through an enzymatic cascade that is similar to, but much simpler than, ubiquitylation. The ATG8 is activated by one ATP-dependent E1 activating enzyme, ATG7, then conjugated with one E2 enzyme, ATG3, and finally coupled to PE via lipidation by an E3 complex composed of an ATG5-ATG12 conjugate and ATG16 (Li & Vierstra, 2012). Modification with ATG8 is essential for closure of the growing phagophores and cargo selections through binding to a large set of ATG8-interacting proteins, including both autophagy adaptors and receptors (Ding et al., 2018; Marshall & Vierstra, 2018). Thus, different to protein ubiquitylation, whose specificity is determined by the pairwise interactions between ubiquitylation substrates and E3 ligases, the specificity of autophagy is primarily determined by ATG8-interacting proteins who bridge ATG8 and autophagy substrates. The large binding capacity of ATG8 could be attributed to its multiple hydrophobic pockets on the surface, such as the AIM/LC3-interacting region docking site (LDS) and the UIM-docking site (UDS) (Marshall et al., 2019; Noda et al., 2010).

To date, the biochemical understanding of many plant UPS and autophagy pathways primarily resulted from studying seedling growth. Given the essential roles of the UPS in the cell cycle and of autophagy in nutrient remobilization, we hypothesized that both systems are indispensable in reproductive development. Consistent with this hypothesis, null mutants of several proteasome subunits have shown various extents of abnormal embryo development. For example, the embryos of the *rpn1a* null mutant are arrested at the globular stage (Brukhin et al., 2005); *rpn5a* shows retarded development with misshaped hypophysis and reduced embryo sizes (Book et al., 2009); and *rpt2a* demonstrates enlarged organs and embryos (Kurepa et al., 2009). Although the null mutant *rpn10-2* is male sterile, *rpn10-1*, which expresses a C-terminally truncated RPN10 fused with a neomycin phosphotransferase (NPT-II) at a declined expression level, is fertile but displays a reduced seed set (Smalle et al., 2003). Unfortunately, none of these studies has addressed in which seed developmental stage(s) the UPS is influential. Despite the fact that seeds, as a major nutrient uptake sink, could easily suffer from nutrient remobilization stress (Guiboileau et al., 2012; Masclaux-Daubresse & Chardon, 2011), only one autophagy mutant, *atg5*, has been studied to date to show varied embryogenesis and abnormal storage protein synthesis (Di Berardino et al., 2018). How autophagy and the UPS work coordinately during seed development is unknown.

During Arabidopsis embryogenesis, the embryonic cells rapidly divide, expand, interact, and differentiate into a wide variety of architectures through a programmable order that can be morphologically divided into dermatogen, globular, heart, torpedo, and mature green stages

(Jenik et al., 2007; Le et al., 2010; Palovaara et al., 2016; Wendrich & Weijers, 2013). Although most genes active in seeds were discovered to be expressed throughout the entire seed development process (Le et al., 2010), distinct transcriptomic phases have been revealed in a recent RNA-Seq-based transcriptome-wide analysis (Hofmann et al., 2019). It remained unexamined whether the UPS is active constitutively or only during a certain stage during seed development. Since autophagy occurs at a background level under nutrient-rich conditions in seedlings (Marshall & Vierstra, 2018; Signorelli et al., 2019), whether this regulation stays the same in seed development is unknown. Given the upregulation of many autophagy genes in Arabidopsis siliques with maturing seeds, autophagy activity was hypothesized to be increased in late seed development (Di Berardino et al., 2018). However, biochemical evidence is yet lacking.

To explore the influence of both the UPS and autophagy on seed development, here, we first confirmed their indispensable roles through identifying varied embryo developmental processes and seed phenotypes in three proteasome and four autophagy mutants. We then compared the expression and activity of the two systems in seedlings, embryos, and young siliques bearing all the key transition stages of Arabidopsis seed development. Our results highlight a reciprocal degradation process between the 26S proteasome and autophagy. The dynamic activity changes allowed us to discover a developmental relay of the UPS and autophagy in maintaining plant proteostasis during early silique and seed development.

RESULTS

Proteasome and autophagy are essential for proper embryo and seed development

To expand our understanding of the role of the proteasome and autophagy in seed development, we used three proteasome and four autophagy mutants (Figure S1a). Through genotyping, protein immunoblotting, and reverse transcription PCR (RT-PCR) analyses, we verified four null (*rpt2a-2*, *atg5-1*, *atg10-1*, and *atg13a-2 atg13b-2*) and three knock-down (*rpn1a-4*, *rpn10-1*, and *atg7-2*) mutants that had been identified in previous studies (Table S1 and Figure S1). Since *rpt2a-2* has enlarged organs and embryos (Kurepa et al., 2009), we compared the seed sizes among the seven mutant lines with wild type (WT). We found that *rpn10-1*, *atg10-1*, and *atg13a-2 atg13b-2* show an enlarged seed phenotype as *rpt2a-2*. However, *rpn1a-4* and *atg5-1* displayed opposite seed phenotypes with seed size similar to or smaller than WT, respectively. Although *atg7-2* did not show significant changes in its seed size, similar to the other three autophagy mutants, it had a larger size variation than WT (Figure S2a–d). After germinating the mutant seeds on half-strength Murashige–Skoog (1/2 MS) medium for 7 days, we discovered that their fully opened cotyledon areas were overall consistent with the seed size phenotype except for *rpn1a-4*, *atg5-1*, and *atg7-2*, whose cotyledons were smaller than, similar to, or larger than WT, respectively (Figure S2e–f).

The seed size variation suggests abnormal embryogenesis. We thus examined the morphology of embryos in siliques 4 days after anthesis (DAA). At this developmental stage, all WT embryos demonstrated a uniform heart shape, which indicates the accomplishment of organ differentiation and basic body patterning, i.e., early embryogenesis (Figure S3a; Lau et al., 2012, Santos-Mendoza et al., 2008). However, all the mutants showed a varied extent of abnormality (e.g., retarded development or abnormal shape) of their embryo morphology, with *rpn1a-4*, *atg5-1*, and *atg13a-2 atg13b-2* having significantly more abnormal embryos than WT ($P < 0.05$, Fisher's exact test; Figure S3b). The enormous impact on embryogenesis and seed size seen in all seven mutants confirmed that both the proteasome and autophagy are essential for proper seed development.

Rapid expression changes of proteasome and autophagy members in early silique and embryo development

Although proteasome and autophagy activities were discovered to be upregulated upon proteotoxic and nutrient starvation stresses, respectively (Gladman et al., 2016; Signorelli et al., 2019), their developmental regulation has barely been studied. The rapid cell fate transition during seed development and the varied proportions of abnormal embryos seen in proteasome and autophagy mutants led us to present a developmentally regulated model of UPS and autophagy activities in seed development. To test this model, we examined both protein abundance and transcript changes of six proteasome subunits and three autophagy members across five different seed developmental transitions, including four early embryogenesis stages representing pre-globular, globular, heart, and late heart embryos and one mature green embryo stage (Figure 1). Embryogenesis analysis in WT suggests that embryos from these stages were developed 1, 2, 3, 4, and 8 DAA under a long-day (LD) photoperiod (Figure 1a). Due to stepwise assembly of the proteasome (Marshall & Vierstra, 2019), we selected two subunits each from the RPN (RPN1 and 12), RPT (RPT2 and 4), and CP (PBA1 and F1) subcomplexes to reflect the changes of the holocomplex. We also utilized the extent of ATG8 lipidation to represent the overall autophagy activities during seed development. Hence, we compared the changes of ATG7, ATG5, and ATG12, all of which are involved in ATG8 lipidation, in parallel with proteasome subunits in the same set of tissues.

Through immunoblotting analysis in siliques (containing seeds, septum, and valves) with different stages of embryos, we unexpectedly discovered an instability of

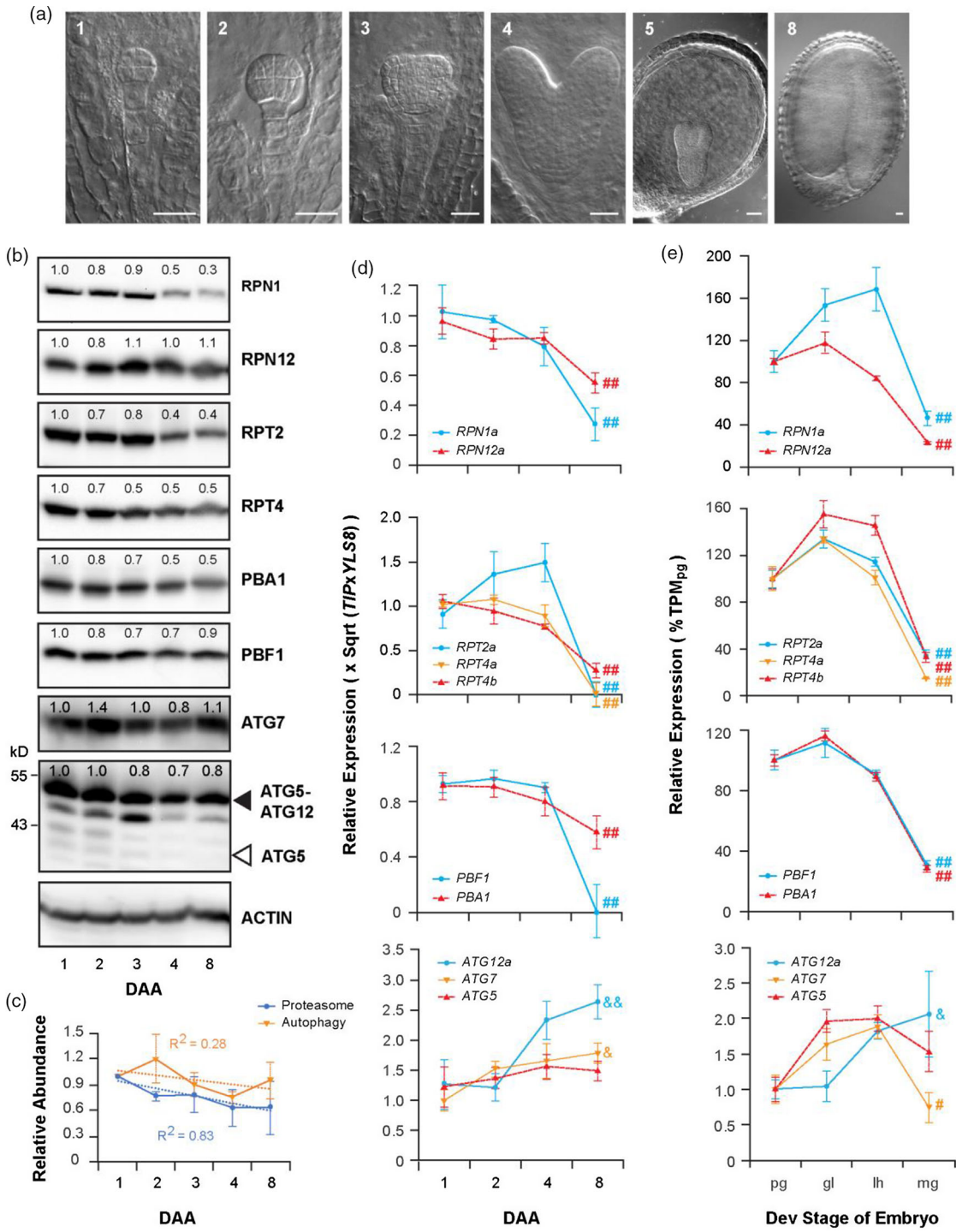

Figure 1. Rapid expression changes of proteasome and autophagy members in early silique and embryo development. (a) Typical stages of embryogenesis seen in siliques developed at the indicated DAA. Scale bar = 20 μm. (b) Immunoblot analysis showing protein abundance changes of selected proteasome and autophagy members in siliques at the indicated DAA. Actin was used to verify nearly equal loading. The number above each band indicates the relative band intensity of an examined protein normalized to actin and to the abundance in 1-DAA siliques. (c) Linear regression analysis confirmed a significant decline in the abundance of proteasome subunits but not autophagy proteins toward silique maturation. Relative abundance is the mean (±SD) of relative band intensities of proteasome or autophagy proteins as detected in (b). (d, e) Transcriptional changes of selected proteasome and autophagy genes in siliques (d) or embryos (e) that were at four indicated seed development stages. Relative expression (mean ± SD) in siliques was normalized to *TIP* and *YLS8* from three biological replicates, each with three technical replicates. Transcripts per million (TPM) values were retrieved from RNA-Seq data (GSE121236; Hofmann et al., 2019). All data points were normalized to one of the three biological replicates from 1-DAA silique (d) or pg embryos (e). pg: pre-globular; gl: globular; lh: late heart; mg: mature green. *P*-values were calculated using Student's *t*-test by comparing the indicated data point with the one from 1-DAA siliques (d) or pg embryos (e). & and &&: P(>1-DAA/pg) < 0.05 and 0.01, respectively; # and ##: P(<1-DAA/pg) < 0.05 and 0.01, respectively.

protein abundance of both proteasome and autophagy members (Figure 1b). The abundance of RPN1, RPT2, RPT4, and PBA1 was reduced by more than half after heart embryos are developed in 4-DAA siliques. The decline of RPN1 is particularly obvious and only a 30% level is retained in 8-DAA siliques compared to those at 1 DAA. A slight decrease in RPN12 and PBF1 levels is also notable in 8-DAA siliques. While the overall abundance of proteasome members clearly declines along seed development ($\rho = -0.9$, $P = 0.05$, Spearman's correlation test), such a trend is not significant for ATG7 and ATG5-ATG12 conjugates ($\rho = -0.6$, $P = 0.4$, Spearman's correlation test; Figure 1c). Instead, their increasing abundance was noticeable in 8-DAA siliques compared to those in 4-DAA siliques (Figure 1b,c).

To examine whether proteasome and autophagy members are under differential transcription regulation in both siliques and embryos, we performed quantitative PCR (qPCR) on siliques and analyzed transcriptome data of isolated embryos from a publicly available RNA-Seq dataset (GSE121236; Hofmann et al., 2019), respectively (Figure 1d,e). Consistent with protein abundance changes, the transcript levels of all six proteasome members decreased dramatically in either 8-DAA siliques or mature green embryos (Figure 1d,e, respectively). However, a continuous rise was detected for the transcripts of three autophagy genes, *ATG5*, *ATG7*, and *ATG12*, in both tissues except for a drop of *ATG7* and *ATG5* transcripts in mature green embryos compared to those in late heart embryos. Mild but noticeable opposite expression changes for proteasome and autophagy genes were detected in siliques as early as 2 DAA. Given the overall anticorrelation of transcript changes between six selected proteasome and three selected autophagy genes (mean Spearman's correlation value, $\rho = -0.69$, Figure S4), we argued that the UPS and autophagy are differentially programmed in silique development.

The 26S proteasome is differentially regulated during development in seedlings and young siliques

The unexpected decline of proteasome expression in both developing siliques and embryos led us to explore its potential regulatory mechanism. Since all the six selected proteasome genes have a consistent >2-fold reduction of their transcript levels in both siliques and embryos toward maturation (Figure 1d,e, respectively), hereafter, we primarily focused on comparison of proteasome activities during development in heart embryo and mature green embryo-containing siliques along with 7-day-old seedlings, all of which were grown under a nutrient-rich condition.

We first examined whether proteasome genes have a reduced response to proteotoxic stress. It is known that the transcription of 46 out of 54 proteasome loci in Arabidopsis is significantly upregulated in seedlings upon 24-h treatment with the proteasome inhibitor carbobenzoxy-Leu-Leu-leucinal (MG132) (Gladman et al., 2016). Interestingly, while we were able to replicate the same result in 7-day-old seedlings, we also detected a similar response of six selected proteasome genes in both 3-DAA and 8-DAA siliques, bearing heart and mature green embryos, respectively, upon 50 μM MG132 treatment in 1/2 MS liquid medium for 24 h (Figure 2a–c). Hence, the reduction of proteasome abundance in young siliques is not likely due to the lack of regulons involved in the proteotoxic response.

We then used the same tissues to examine the changes in protein abundance. Again, we saw an increase in the protein levels of all six proteasome subunits in 7-day-old seedlings treated with MG132, which was consistent with transcription upregulation (Figure 2d; Gladman et al., 2016). However, a disconnection between transcript and protein levels in response to MG132 treatment was observed in silique tissues. While only a slight increase was detected for RPN1, RPT2, and RPN12 in 3-DAA siliques treated with MG132, the levels of the RPN proteins RPN1 and RPN12 and PBF1 declined in 8-DAA siliques upon MG132 treatment (Figure 2d). This distinct response to MG132 is consistent with the changes of proteasome activities. The proteasomes isolated from 3-DAA siliques have a slightly but significantly lower activity than those from 7-day-old seedlings. Unexpectedly, they better tolerated the suppression of MG132, suggesting the presence of differential structural assembly of proteasomes between seedlings and young siliques (Figure 2e). Consistent with the significant reduction of subunit abundance (Figures 1d and 2d), proteasome activities in the extracts of 8-DAA siliques were only 15% of those of 3-DAA siliques but responded to MG132 treatment more mildly (Figure 2e).

Opposite activity regulation of protein ubiquitylation and autophagy across silique and embryo development

The dramatic decline of proteasome activity and expression upregulation of autophagy members in 8-DAA mature green embryo-containing siliques suggests a differential activity regulation of the UPS and autophagy in seed development. We therefore utilized protein ubiquitylation and ATG8 lipidation to monitor their activity changes.

Similar to the transcript changes of six proteasome genes, the total transcript levels of nine poly-*UBQ* genes (containing at least three *UBQ* moieties; Hua et al., 2018) showed a declining, albeit statistically not significant, trend upon maturation of embryos. However, those of nine *ATG8* homologs increased significantly (Figure 3a and Table S2). We further analyzed by qPCR the transcript changes of the top four transcriptionally active members from each family in siliques at different developmental stages. Similar trends were evident. While the transcript levels of *UBQ* genes did not show a statistical difference

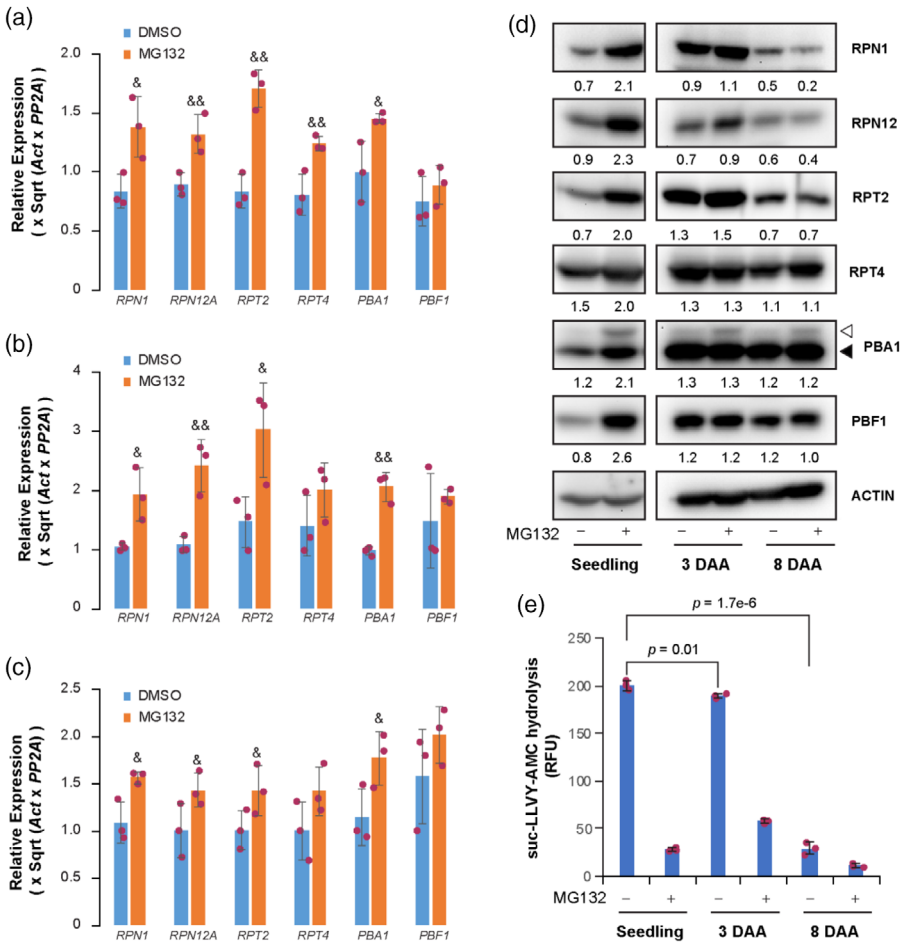

Figure 2. Proteasome activity is distinctly regulated in seedlings and developing siliques. (a–c) Expression of six selected proteasome genes was consistently upregulated upon MG132 treatment in 7-day-old seedlings (a) and 3-DAA (b) and 8-DAA (c) siliques. Expression of each gene was normalized to one of the three biological replicates treated with the solvent dimethyl sulfoxide (DMSO) only. *ACT2* and *PP2A* were used as reference standards. Bars represent the mean (±SD) from three biological replicates, each with three technical replicates. The data points of replicates in each bar are indicated with maroon dots in these panels as well as others throughout the paper. (d) Protein abundance of selected proteasome subunits responds to MG132 treatment distinctly among 7-day-old seedlings and 3-DAA and 8-DAA siliques. Proteins extracted from the same set of tissues as in (a–c) were used for the immunoblot assay with antibodies against each subunit. The efficacy of MG132 treatment is judged by accumulation of the PBA1 precursor (open arrowhead) upon proteasome inhibition (Book et al., 2010). The number below each band indicates the relative band intensity that was normalized to actin. (e) Proteasome activities decline rapidly in developing siliques but tolerate MG132 treatment better than in seedlings. Total protein extracts were assayed for proteasome activities based on the fluoresce intensity of 7-amido-4-methylcoumarin (AMC) after cleavage from the substrate succinyl-leucyl-leucyl-valyltyroyl-7-amido-4-methylcoumarin (suc-LLVY-AMC). Bars represent the mean (±SD) of three biological replicates, each with three technical replicates. *P*-values were calculated using Student's *t*-test.

across the four samples, *ATG8* genes, particularly *ATG8F*, *ATG8G*, and *ATG8H*, were upregulated >4-fold in mature green embryo-bearing siliques compared to the early developmental siliques with pre-globular or globular embryos (Figure 3b).

Given the consistent transcript changes of *UBQ* and *ATG8* genes in developing embryos and siliques (Figure 3a,b, respectively), we further compared the biochemical changes of protein ubiquitylation and ATG8 lipidation in young siliques. Previous studies have demonstrated that the products of the *GFP-ATG8* transgene are lipidated, like endogenous ATG8, through the autophagy lipidation pathway in both yeast and plant cells (Chung et al., 2010; Marshall et al., 2019; Nair et al., 2011). Hence, we monitored the rates of both protein ubiquitylation and GFP-ATG8a lipidation in a series of eight young silique samples whose developmental ages precisely differed one day (Figures 3c,d and S5). After normalizing total ubiquitylated protein abundance to actin in each sample, a slight upregulation in 2-DAA siliques followed by a constant decline onward is evident ($\rho = -0.8$, $P = 0.02$, Spearman's correlation test; Figure 3e, top panel). Although the total abundance of GFP-ATG8a decreases due to reduced activity of the 35S promoter during seed maturation (Huang et al., 1994), the ratio of free GFP to GFP-ATG8a indeed constantly increases in siliques toward maturation

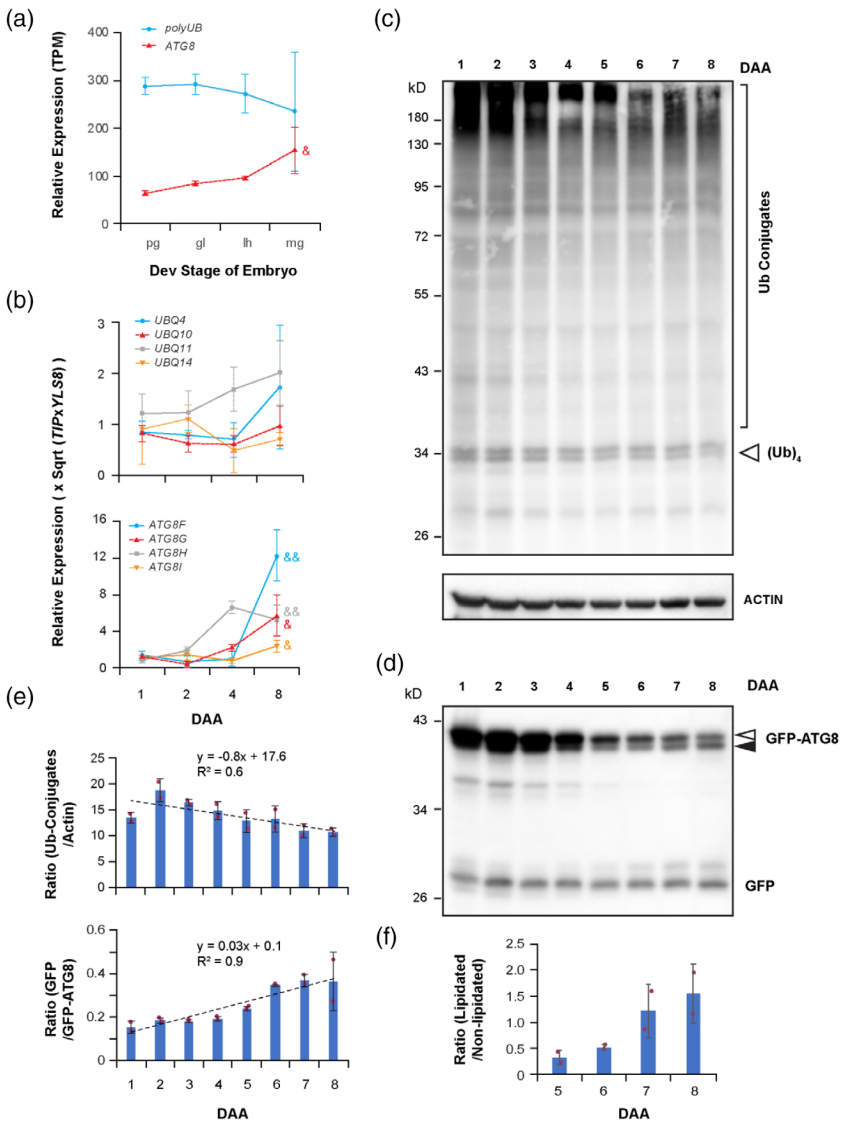

Figure 3. A timeline of protein ubiquitylation and autophagy flux in developing siliques. (a) Total transcript levels change inversely between the *UBQ* and *ATG8* gene families during embryogenesis. Relative expression was calculated based on the total transcripts per million (TPM) values of nine members from each family as described in Table S2. Each data point represents the mean (±SD) from three biological replicates. *P*-values were calculated and indicated as in Figure 1e. (b) The expression of *ATG8* but not *UBQ* genes is gradually upregulated in siliques toward maturation. Top four transcriptionally active members from each family as determined in panel (a) were selected for the analysis. Relative expression of each indicated gene and *P*-values were calculated as in Figure 1d. (c) The abundance of total ubiquitylated proteins gradually declines in siliques upon maturation. Siliques at eight different developmental stages with 1 day difference were harvested from *35S:GFP-ATG8a* transgenic plants (Thompson et al., 2005) and extracted for protein immunoblot analysis using anti-Ub antibodies. Actin was used as a control indicating nearly equal protein loading. (d) Increasing autophagy flux in developing siliques upon maturation. The same set of protein samples prepared in (c) was used for the immunoblotting assay with antibodies specific to GFP. Open and solid arrowheads indicate free and lipidated GFP-ATG8a, respectively, as verified in Figure S5d. (e) Quantitative analysis demonstrates inverse activity changes between protein ubiquitylation and autophagy flux. The abundance of total ubiquitylated proteins is normalized to actin in each sample. The autophagy flux is represented by the ratio of free GFP to GFP-ATG8a as previously assayed (Marshall et al., 2015). Bars represent the mean (±SD) of two independent biological replicates as shown in (c, d) and Figure S5b,c. (f) Increasing lipidation of GFP-ATG8a in siliques from 5 DAA toward maturation. The ratio of the lipidated form to the free GFP-ATG8a is calculated based on the band intensities as shown in panel (d) and Figure S5c. Bars are as indicated in panel (e).

(ρ = 0.95, P = 0.001, Spearman's correlation test; Figure 3e, bottom panel). Because autophagy-mediated proteolysis in vacuoles leads to the cleavage of GFP from GFP-ATG8a, the higher the ratio of free GFP to GFP-ATG8a is, the higher is autophagic activity (Marshall et al., 2015).

The upregulated autophagy flux is further confirmed by the increase of a faster migrating species of GFP-ATG8a evident from 5-DAA siliques onward (Figures 3d,f and S5c). Because PE-conjugated ATG8 forms migrate faster than free ATG8 proteins in SDS-PAGE (Ichimura

et al., 2000), we predicted this faster migrating GFP-ATG8a is GFP-ATG8a-PE. Interestingly, upon phospholipase D (PLD) treatment, it disappeared in a membrane fraction prepared from 8-DAA siliques while it was retained in the membrane fraction without PLD treatment, indicating its delipidation by PLD (Figure S5d, upper panel). We also examined the mobility changes of native ATG8 and ATG8-PE forms in the same set of samples. While a majority of the soluble fraction is detected as ATG8, the membrane fraction contained both ATG8 and ATG8-PE. Because both ATG8-PE and GFP-ATG8a-PE disappeared in the same membrane fraction treated with PLD (Figure S5d, bottom panel), we confirmed that they were delipidated by PLD. GFP-ATG8a and GFP-ATG8a-PE were also similarly detected in a previous study on nitrogen-starved seedlings (Chung et al., 2010). The linear increase of the GFP/GFP-ATG8 ratio and the accumulation of GFP-ATG8a-PE suggest that autophagy is gradually upregulated toward silique maturation.

To further demonstrate the upregulation of autophagy during silique development, we examined the developmental-dependent changes of Next to BRCA1 (NBR1) in WT siliques from 1 DAA to 8 DAA. NBR1 is both a receptor and a substrate of autophagy degraded in the vacuole (Svenning et al., 2011). Interestingly, we discovered a nearly linear reduction of NBR1 from 1-DAA to 8-DAA siliques ($\rho = -0.7$, $P = 0.05$, Spearman's test; Figure 4a,b). qPCR analysis shows a relatively stable mRNA level of *NBR1* from 1-DAA to 4-DAA siliques as well as in 8-DAA siliques (Figure 4c), in which the protein abundance has reduced 7-fold compared to that in 3-DAA siliques (Figure 4b), suggesting a developmental-dependent degradation of NBR1. Since the activities of vacuole-resident proteases are suppressed by the rise of vacuolar alkalinization, which can be achieved by treatment with the V-ATPase-specific inhibitor concanamycin A (ConA; Huss et al., 2002), we further compared the stability changes of NBR1 in 3-DAA and 8-DAA siliques treated with 1 μM ConA for 24 h (Figure 4d). Consistently, 1.2 ± 0.2 and 2.0 ± 0.5 (mean ± SD) fold more NBR1 proteins were detected in 3-DAA and 8-DAA siliques, respectively, upon ConA treatment (Figure 4e). The significantly more NBR1 stabilized by ConA in the latter tissue further implies increased autophagy activity (Figure 4e).

Taken together, our data demonstrate an opposite activity regulation of protein ubiquitylation and autophagy across silique and/or embryo development.

Upregulation of autophagy results in non-selective proteasome degradation in developing siliques

The proteasome has been found to be selectively degraded by autophagy upon proteotoxic damage (Marshall et al., 2015). Based on the significant reduction in the levels of six selected proteasome subunits and the upregulation of autophagy in silique and/or embryo development, we investigated whether the proteasome could be degraded by autophagy upon silique development. We compared the protein abundance of the same set of six proteasome subunits as in Figures 1 and 2 in 3- and 8-DAA siliques from WT and the *atg7-2* mutant (Figure 5). We again observed reduced protein levels of these subunits to different extents upon silique maturation in WT. In particular, the abundance of RPN1, RPN12, and RPT2 in 8-DAA siliques is statistically significantly lower than that in 3-DAA siliques based on their relative abundance detected in 10 independent biological replicates ($P < 0.01$, Student's *t*-test; five replicates each in Figures 5a and S6). However, except for RPN1, such developmental reductions were nearly eliminated in *atg7-2* (Figure 5a). Consequently, a significantly higher abundance of proteasome subunits, such as RPN12, RPT2, PBA1, and PBF1 ($P < 0.01$, Student's *t*-test), was detected in 8-DAA siliques from *atg7-2* than that from WT, whereas none showed significantly higher transcript levels in *atg7-2* than in WT (Figures 5 and S7). Collectively, these results suggest that the proteasome is subject to autophagy degradation in developing siliques.

To test whether this degradation involves an RPN10-mediated selective proteaphagy pathway (Marshall et al., 2015), we further compared their abundance between WT and the *rpn10-1* mutant. Contrastingly, they did not show any obvious difference with regard to both steady-state levels and developmental changes of all six subunits, except for a significant reduction of RPN1 in 8-DAA siliques from *rpn10-1* (Figure S6). Thus, the proteasome is likely targeted for autophagy-mediated non-selective degradation in silique development. To confirm this bulk degradation, we treated 3- and 8-DAA siliques from WT with ConA to examine whether proteasome subunits, like NBR1 (Figure 4d,e), could be stabilized. After 24-h treatment, an increased abundance of all tested proteasome subunits except for RPN1 was either evident or statistically significant (RPT4 and PBF1; $P = 0.02$, Student's *t*-test) in 8-DAA siliques upon ConA treatment (Figure S8).

ATG5, ATG5-ATG12 adducts, and ATG7 are targeted by the UPS for degradation in seedlings and young siliques

It was previously discovered that ATG12 is degraded in a UPS-dependent manner in human cells (Haller et al., 2014). Recently, ATG13 was also shown to be targeted for UPS-mediated turnover in Arabidopsis seedlings under a normal nutrient-rich condition (Qi et al., 2020). The opposite activity regulation between the UPS and autophagy in developing siliques led us to hypothesize that the autophagy is targeted by the UPS in seedlings and during early silique development. We thus examined the stability changes of ATG5, ATG7, and ATG12, three key autophagy members involved in ATG8 lipidation, in both seedlings

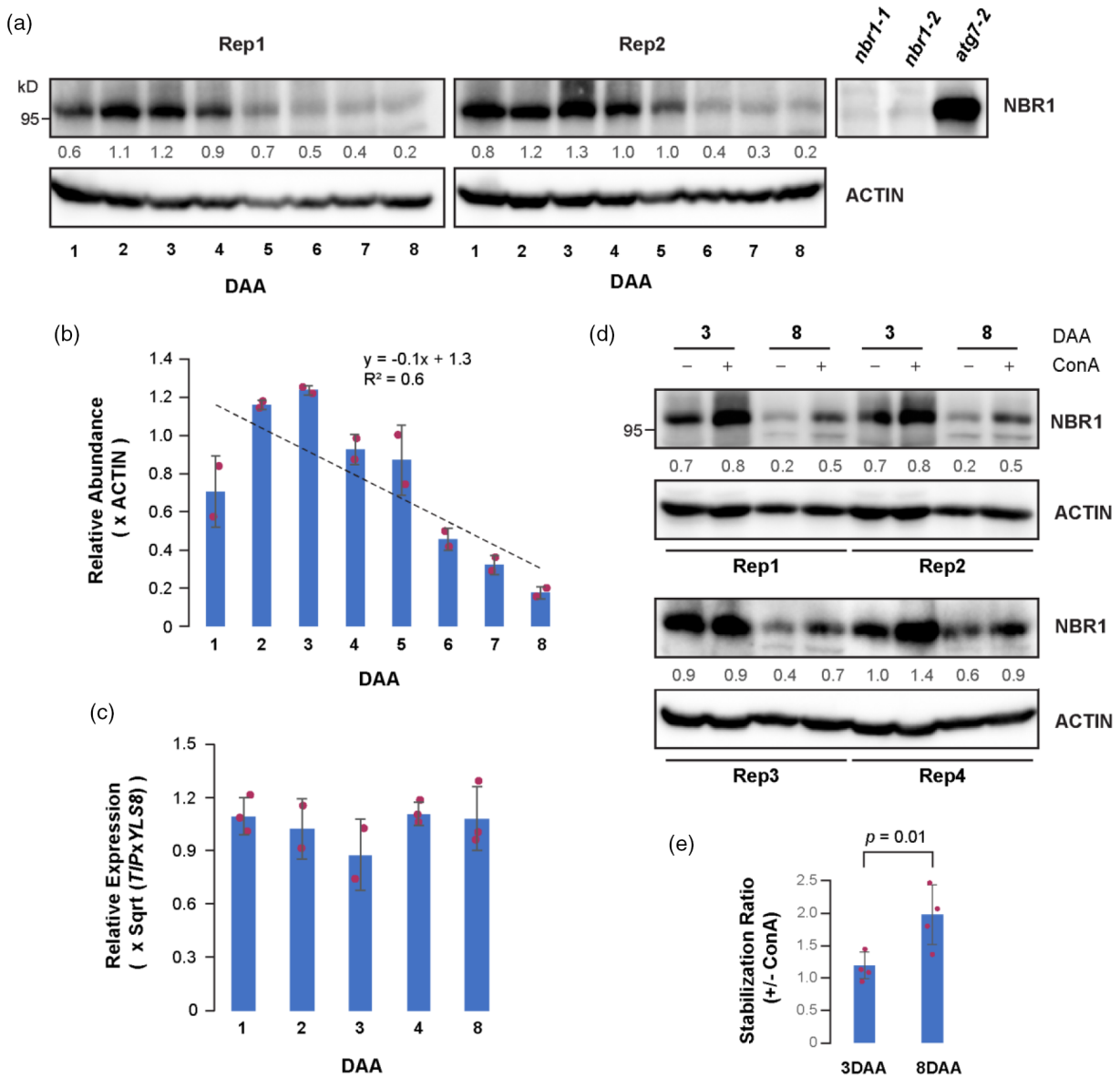

Figure 4. Stability changes of NBR1 indicate linear upregulation of autophagy in early silique development. (a) Immunoblot analysis of NBR1 in a collection of successive WT siliques that differed 1 day. The T-DNA insertion mutants *atg7-2* and *nbr1-1/2* were used to indicate the presence and absence of NBR1, respectively (Jung et al., 2020). Actin was used to normalize the relative abundance of NBR1 labeled below each sample as in Figure 2d. (b) Linear regression assay of NBR1 abundance during silique development. (c) The transcription of *NBR1* does not change dramatically during silique development. Relative expression (mean ± SD) in siliques with indicated developmental stages was analyzed as in Figure 1d. (d) NBR1 is stabilized in siliques upon ConA treatment. Four independent biological replicates from 3- and 8-DAA siliques were used to examine the stability of NBR1. Relative abundance of NBR1 labeled below each sample was calculated as in panel (a). (e) Quantitative assay indicating that ConA treatment stabilizes NBR1 more effectively in 8-DAA siliques than in 3-DAA siliques. The *P*-value was calculated by Student's *t*-test using the relative abundance of NBR1 detected in panel (d).

and siliques from WT upon MG132 treatment. Because the majority of ATG5 and ATG12 proteins are conjugated together by ATG3 (Li & Vierstra, 2012), we used ATG5-ATG12 adducts to monitor their stability in response to MG132 treatment. Consistent with our hypothesis, we detected that free ATG5 and ATG7 were stabilized by MG132 in 7-day-old seedlings and 3-DAA siliques but not in 8-DAA siliques, indicative of UPS-mediated degradation in young tissues (Figures 6a and S9). The stabilization of ATG5-ATG12 adducts was detected more significantly in seedlings than in siliques (Figure S9b), indicating differential UPS-mediated regulation. No increases in transcript levels were detected in these tissues in response to MG132 treatment, further confirming their post-translational degradation (Figure S10). To further demonstrate UPS-mediated regulation of ATG7, we immunoprecipitated it

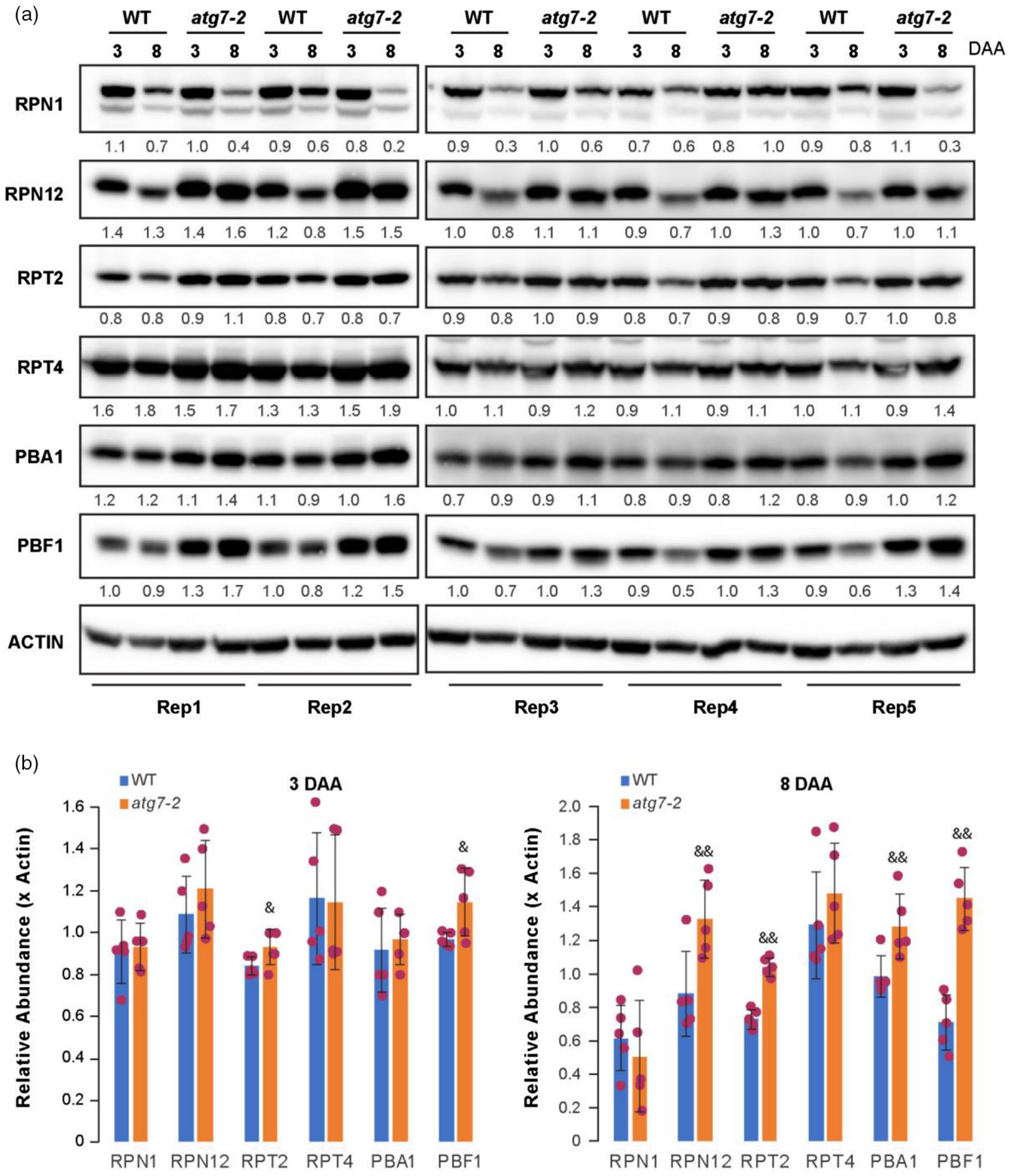

Figure 5. Bulk autophagy-mediated degradation of proteasome subunits. (a) Parallel immunoblot assay showing both abundance upregulation and elimination of developmental reduction for five out of six selected proteasome members in *atg7-2* siliques. Siliques at 3 and 8 DAA collected at the same time from WT and *atg7-2* were extracted for the assay. Five independent biological replicates were analyzed. Actin was used to normalize the relative protein abundance as in Figure 2d. (b) Normalization assay confirming upregulation of selected proteasome members except for RPN1 in *atg7-2*, particularly in 8-DAA siliques. Relative abundance of an indicated proteasome subunit in each sample was calculated by normalizing its band intensity to actin as detected in panel (a). Left panel: 3-DAA; right panel: 8-DAA. Bars represent the mean (±SD) of five biological replicates as shown in panel (a).

out of the protein extracts from 7-day-old seedlings and 3-DAA siliques and detected ubiquitylated species more strongly in samples treated with MG132 (Figures 6c and S11, respectively). Collectively, our data suggest a UPS-mediated suppression of ATG8 lipidation in young tissues, including seedlings and early immature siliques.

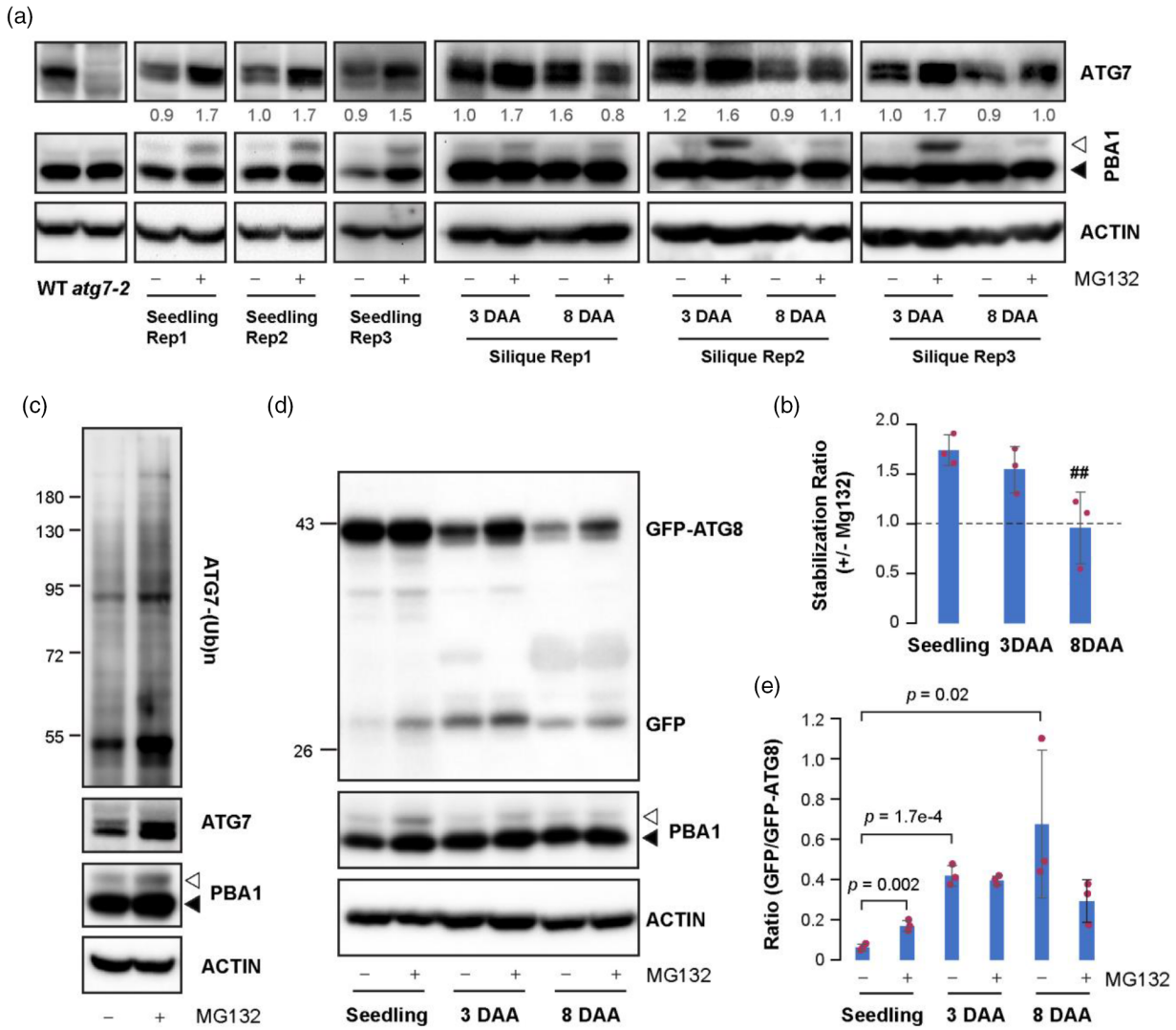

Figure 6. Upregulation of autophagy in developing siliques is in part attributed to reduced degradation of autophagy members by the UPS. (a) ATG7 is degraded in a UPS-dependent manner in 7-day-old seedlings and 3-DAA siliques but not in 8-DAA siliques. Samples from each tissue were treated as in Figure 2(d) and extracted for an immunoblot assay using antibodies against ATG7. Immunoblot analysis with anti-PBA1 antibodies demonstrated the efficacy of MG132 treatment as described in Figure 2(d). Actin was used to normalize the relative abundance of ATG7 marked below each sample. (b) Quantitative assay confirming reduction and elimination of UPS-mediated ATG7 degradation in 3- and 8-DAA siliques, respectively. The UPS-mediated ATG7 degradation in each tissue is measured as the ratio of ATG7 abundance identified in samples treated with or without MG132. Bars represent the mean (±SD) of three biological replicates as shown in (a). *P*-values were calculated using Student's *t*-test. (c) ATG7 is ubiquitylated in 7-day-old seedlings. The same set of 7-day-old seedling samples prepared as in panel (a) was used for protein extraction with a ubiquitylation immunoprecipitation buffer. ATG7 proteins were then immunoprecipitated with anti-ATG7 and examined for ubiquitylation with anti-Ub. The high-molecular weight species indicate the ubiquitylated forms of ATG7. More ATG7 proteins identified to be ubiquitylated and stabilized upon MG132 treatment confirm its UPS-mediated degradation. PBA1 is used as a control indicating the efficacy of MG132 treatment as described in Figure 2(d). Actin staining indicates an equal amount of protein extract was used for ATG7 immunoprecipitation. (d) Immunoblot analysis showing the changes of vacuolar breakdown of GFP-ATG8a in 7-day-old seedlings and 3- and 8-DAA siliques upon MG132 treatment. Both free GFP and GFP-ATG8a were detected by anti-GFP antibodies. PBA1 and actin were used as controls as described in panel (c). (e) Quantification of the ratio of free GFP to GFP-ATG8a following MG132 treatment. Bars represent the mean (±SD) of three biological replicates as shown in Figure S12. Statistically significant differences are indicated by the *P*-values calculated based on Student's *t*-test.

UPS-mediated autophagy suppression is compromised in developing siliques

Given the discovery of UPS-mediated degradation of ATG5, ATG5-ATG12 adducts, ATG7, and ATG13 (this work and Qi et al., 2020), we hypothesized that the autophagy activity is dampened by the UPS in plants under normal growth. Since MG132 increased the stability of ATG5 and ATG7 in 7-day-old seedlings and 3-DAA siliques but not in 8-DAA siliques after 24-h treatment (Figures 6 and S9), we compared the breakdown efficiencies of GFP-ATG8a in these tissues. We first detected a robust increase of the GFP/GFP-ATG8a ratio in seedlings treated with MG132,

confirming the UPS-mediated negative regulation of autophagy activities (Figures 6d,e and S12a). However, we did not observe such an upregulation in 3- and 8-DAA silique samples upon MG132 treatment, whereas the ratio of GFP/GFP-ATG8a in both silique samples was >10-fold higher than that in seedlings without MG132 treatment (Figures 6e and S12b). The ratio of free GFP to GFP-ATG8a slightly declined, albeit not statistically significantly, in 8-DAA siliques if treated with MG132 for 24 h (Figure 6e). The inability to increase GFP/GFP-ATG8a ratios in siliques by MG132 treatment could be a combined effect of (i) differential regulation and weakened proteasome activities (Figure 2), (ii) declined ubiquitylation processes (Figure 3e), and (iii) significantly enhanced autophagy activities (Figures 3e, 4b, and 6e). Consequently, the suppression of autophagy by the UPS in siliques, particularly in maturing siliques, is too mild to be changed by MG132 treatment under the background of high autophagy activities.

A significant increase in GFP-ATG8a levels upon MG132 treatment was noticeable in both 3-DAA and 8-DAA siliques (Figure S12b), suggestive of another unknown regulatory pathway by the UPS. Conversely, ConA treatment either did not influence or reduced the abundance of GFP-ATG8a significantly in 3-DAA and 8-DAA siliques, respectively, while it increased the ratio of GFP/GFP-ATG8a in all three tissues examined (Figure S13). The increase of the GFP/GFP-ATG8a ratio could result from proteolysis suppression of free GFP in the vacuole in both seedlings and 3-DAA siliques in a way as previously reported in seedlings (Marshall et al., 2015), or by accelerating the reduction of GFP-ATG8a in 8-DAA siliques (Figure S13b). How MG132 and ConA impact the stability changes of GFP-ATG8a in siliques and whether these impacts reflect the changes of endogenous ATG8 proteins require further investigation.

DISCUSSION

Seed development involves multiple intricate reprogramming events through cell division and expansion, cell–cell interactions, and cell fate specification (Sreenivasulu & Wobus, 2013; Wendrich & Weijers, 2013). These events include embryogenesis, growth and degeneration (or programmed cell death in monocotyledon plants) of endosperm, seed coat formation from the maternal integument tissues, deposition of reserves during seed maturation, and seed desiccation (Dure III, 1975). In Arabidopsis, these processes are accomplished in a short period of its entire life cycle. For example, embryogenesis takes place only 8 days after fertilization (Figure 1a). Given both scientific and agronomic values, many efforts have been made to understand the molecular mechanisms underpinning seed development (see reviews in Dresselhaus & Jurgens, 2021; Jenik et al., 2007; Leprince et al., 2017; Palovaara et al., 2016; Santos-Mendoza et al., 2008). However, in contrast to the discoveries of many transcription factors that regulate different stages of seed development (Holdsworth et al., 2008; Lau et al., 2012; Leprince et al., 2017), the involvement of proteostasis regulation is just starting to be appreciated (Di Berardino et al., 2018; Guiboileau et al., 2012; Li et al., 2015; Sreenivasulu & Wobus, 2013). In this work, we took advantage of a suite of biochemical and genetic materials and systematically compared the activities of both proteasome- and autophagy-mediated protein degradation pathways in seedlings and developing siliques and/or embryos under a normal nutrient-rich growth condition. Our results indicate several previously unnoticed features of the two systems in developing siliques or embryos that differ from their functions in seedlings.

First, the activity of the proteasome but not autophagy is downregulated rapidly by transcriptional regulation in early silique and/or embryo development (Figure 1). The overall consistent declines in transcript levels of selected six proteasome members in embryos and their bearing siliques suggest the presence of a yet unknown transcription suppression program that is commonly triggered by fertilization in both maternal and embryonic tissues. This is exciting about the functional regulation of the proteasome. Previous studies discovered a positive upregulation of proteasome expression by NAM, ATAF, and CUC (NAC) transcription factors in seedlings upon proteotoxic stress induced by MG132 treatment (Gladman et al., 2016). Consistently, we also observed this process in siliques carrying both immature and mature green embryos (Figure 2a–c). However, the latter tissue has dramatic low levels of proteasome transcripts and activities (Figures 1d,e and 2e, respectively), which indicate their transcriptional downregulation is not likely due to NAC transcription factors. Instead, a seed development-specific transcriptional reprogramming is likely involved. The discovery of this pathway will further our understanding of the molecular events in early seed development.

In contrast to the proteasome, the members involved in ATG8 lipidation are slowly transcriptionally upregulated in early embryogenesis followed by a sharp rise for some members toward mature green embryos such as *ATG12a* and *ATG8F* (Figures 1d,e and 3b, respectively). Similar to the proteasome members, the transcriptional regulation of autophagy members is also consistent in both siliques and isolated embryos. It is yet unknown whether a universal program is applied to regulate proteasome and autophagy in an opposite manner. Given the maintenance of a similar (albeit significantly reduced) proteasome activity but an approximately 10-fold upregulation of autophagy functions in 3-DAA siliques when compared to seedlings (Figures 2e and 6e, respectively), it is likely that these two systems are separately reprogrammed during seed development.

The strong upregulation of autophagy in developing siliques expands its developmental roles even under nutrient-

rich conditions. Previous studies in maize (*Zea mays*) have indicated the increase of autophagy in both embryo and endosperm tissues toward late seed development (Chung et al., 2009). While our study in Arabidopsis echoed this biochemical feature of autophagy in seed development, we believe that autophagy is rapidly upregulated during early silique development based on our comparison of autophagy gene transcript levels, our GFP breakdown assay of GFP-ATG8a, and the degradation of NBR1 in siliques that bear the entire process of embryogenesis (Figures 1d,e, 3d–f, and 4, respectively). This rapid upregulation is also in part attributed to the downregulation of UPS-mediated degradation of key autophagy members. In addition to the previous discovery of ATG13 degradation, we expanded the list of UPS substrates to three key enzymes, ATG5, ATG7, and ATG12, that are involved in ATG8 lipidation, the rate-limiting step in autophagy (Figures 6a–c and S9). Similar to ATG13, the degradation of ATG7 and ATG5 is more prominent in seedlings that are well fed with nutrients compared to 8-DAA siliques (Figures 6b and S9b). Intriguingly, the rise of autophagy results in the bulk degradation of proteasomes in siliques (Figures 5, S6, and S8). Therefore, while both the proteasome and autophagy are likely reprogrammed separately by transcriptional regulation, they are also intimately connected by targeting each other for turnover in an arms race manner throughout plant growth and development.

In summary, we proposed a relay model for the roles of the proteasome and autophagy in regulating proteostasis during silique and likely also during embryo development (Figure 7). Since it takes time for transcriptional reprogramming to be effective, the gradually decreasing and increasing activities of proteasome and autophagy, respectively, in silique and/or embryo development disrupted their arms balance. While the proteasome remains active in early embryogenesis accommodating the need for rapid protein turnover in cell division and differentiation, the accomplishment of organ differentiation and basic body patterning at the end of early embryogenesis (heart stage in Arabidopsis) significantly reduces the need of this regulatory process. Instead, autophagy-mediated bulk degradation allows the filling of nutrients in the growing embryo and promotes degeneration or programmed cell death in endosperm. To meet the seamless connection of both degradation pathways, autophagy genes are upregulated as early as the proteasome genes are downregulated. Taken together, our studies highlights a developmental interplay of the two large protein degradation pathways in plants.

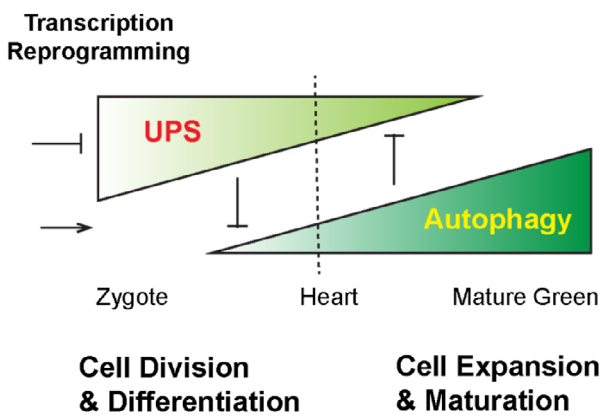

Figure 7. A relay model of the regulatory functions of UPS and autophagy during silique and/or seed development. Upon fertilization, the transcription reprogramming suppresses and activates the UPS subunits and autophagy proteins, respectively, in both embryos and maternal tissues. During early embryogenesis (heart embryo stage), slow downregulation of the UPS allows it to be active enough for regulating cell division and differentiation but with a compromised function in degrading autophagy members. Arising expression of autophagy proteins outcompetes the degradation activity of the UPS in late embryogenesis toward maturation. Its bulk degradation of proteasomes further reduces the UPS activities.

EXPERIMENTAL PROCEDURES

Plant materials, growth, and treatment

The Arabidopsis reference accession Col-0 was taken as the WT control. Accession numbers and genotyping primers of proteasome and autophagy mutants are listed in Tables S1 and S3, respectively. Seeds harvested at the same time from plants grown under the same condition were synchronized by stratification in water at 4°C for 3 days before germinating on 1/2 MS medium (Caisson Labs, Smithfield, UT, USA) containing 1% (w/v) sucrose and 0.7% (w/v) agar. Seven-day-old seedlings were then plotted in mixed soil containing 1/3 vermiculite, 1/3 peat moss, and 1/3 compost soil. Unless otherwise noted, seedlings on plates or plants on soil were germinated and grown under an LD photoperiod with 16 h light (125 μmol m^{-2} sec^{-1}) and 8 h darkness at 21°C and 19°C, respectively. Adult plants in soil were fertilized once before bolting with 0.1% (w/v) 20–20-20 (Miracle-Gro, Marysville, OH, USA), calcium nitrate (0.17 mM), and magnesium sulfate (0.33 mM). Both MG132 (50 μM; Cell Signaling Technology, Danvers, MA, USA) and ConA (1 μM; BioViotica, Dransfeld, Germany) treatments on 7-day-old seedlings or 3- and 8-DAA siliques were performed in 1/2 MS liquid medium containing 1% (w/v) sucrose for 24 h under an LD photoperiod with shaking at 150 rpm. Samples were vacuum-infiltrated for 20 min every 8 h of incubation.

Analysis of embryogenesis

Siliques formed naturally at various DAAs were labeled, collected, dissected, immersed directly in a drop of Hoyer's Solution (chloral hydrate:glycerol:water = 8:1:2, w/v/v) (Anderson, 1954), and incubated for 24 h. Cleared ovules were photographed using differential interference contrast optics on a Nikon Eclipse E600 microscope.

Immunoblot analysis

Tissues were harvested, frozen in liquid nitrogen, and temporarily stored in a −80°C freezer before analysis. Unless otherwise noted, total protein from pulverized tissues was directly extracted in SDS-PAGE sample buffer. After SDS-PAGE, proteins were electrophoretically transferred onto polyvinylidene difluoride membranes (Immobilon-P; Millipore Sigma, St. Louis, MO, USA).

Antibodies against selected proteasome and autophagy members were used as previously described (Huang et al., 2019; Marshall et al., 2015; Thompson et al., 2005). Anti-β-actin, anti-GFP, and anti-Ub were obtained from Proteintech, Abcam, and Santa Cruz Biotechnology (Dallas, TX, USA), respectively. Antibody concentrations are listed in Table S4. Band intensity was quantified by densitometric scans of immunoblots using ImageQuant5.2 (GE Healthcare, Cleveland, OH, USA).

RNA isolation and qPCR analysis

Total RNA was isolated from tissues using the NucleoSpin RNA kit (Macherey-Nagel, Düren, Germany) according to the manufacturer's instructions. Three independent biological samples were prepared. cDNA was synthesized from 1.5 μg of total RNA with SuperScript III (Thermo Fisher Scientific, Asheville, NC, USA) and used as template for qPCR with PowerUp™ SYBR™ Green Master Mix (Thermo Fisher Scientific) according to the manufacturer's instructions. Reactions of all samples were run with technical triplicates on a Bio-Rad CFX Connect™ real-time system (Bio-Rad, Hercules, CA, USA). Relative gene expression was calculated according to the $2^{-\Delta\Delta Ct}$ method with *YLS8* and *TIP* or *ACT2* and *PP2A* pairs as internal controls. Primers for all qPCR reactions are listed in Table S3.

Proteasome activity assay

After extraction in lysis buffer (50 mM Tris–HCl, pH 7.5, 5 mM $MgCl_2$, 1 mM Na_2EDTA, 10% [v/v] glycerol), 10 μg total protein, as determined by a Bradford assay (Bio-Rad), from each clarified extraction was used for the assay as previously described (Marshall et al., 2015; McLoughlin et al., 2019). Briefly, the same amount of protein extract from each sample in a volume of 20 μl was incubated for 20 min at 37°C in 1 ml assay buffer (50 mM Tris–HCl, pH 7.0, 2 mM $MgCl_2$, 1 mM ATP, 2 mM β-mercaptoethanol) containing 100 μM N-succinyl-leucyl-leucyl-valyl-tyrosyl-7-amino-4-methylcoumarin (suc-LLVY-AMC, Sigma-Aldrich) in the presence or absence of 50 μM MG132. Upon incubation, the reaction was quenched by mixing with 1 ml of 80 mM sodium acetate (pH 4.3). The fluorescence resulting from the released AMC was recorded in a TKO 100 fluorometer (Hoefer Scientific Instruments, Holliston, MA, USA) with an excitation wavelength of 365 nm and an emission wavelength of 460 nm. Three biological replicates each with three technical replicates were assayed.

ATG8 delipidation assay

The ATG8 delipidation assay was carried out as described previously (Chung et al., 2010). Briefly, 8-DAA siliques from *35S:GFP-ATG8* transgenic plants were collected and extracted in extraction buffer (EB) containing 50 mM Tris–HCl, pH 8.0, 150 mM NaCl, 1 mM phenylmethanesulfonylfluoride, and 10 mM iodoacetamide. The crude extract was clarified by centrifugation at 2000 ***g*** for 5 min at 4°C. The resulting supernatant was further centrifuged at 100 000 ***g*** for 1 h to obtain the membrane fraction, which was redissolved in EB supplemented with 0.5% (v/v) Triton X-100. The solubilized membrane proteins were incubated for 1 h at 37°C in the presence or absence of 250 units ml^{-1} *Streptomyces chromofuscus* PLD (Enzo Life Sciences, Farmingdale, NY, USA). All protein samples were denatured in SDS-PAGE sample buffer and resolved by 4–20% SDS-PAGE for immunoblot analysis.

ATG7 ubiquitylation analysis

First, 100 mg 7-day-old WT seedlings or 3-DAA siliques treated with or without MG132 was extracted with 200 μl ubiquitylation immunoprecipitation buffer (10 mM iodoacetamide, 10 mM sodium metabisulfite, 10 mM 2-chloroacetamide, 1× plant protease inhibitor cocktail [Millipore Sigma], 1 mM PMSF, and 50 μM MG132 in 1× Tris-buffered saline plus 0.1% Tween® 20 [TBST]). Anti-ATG7 antibodies (5 μl) were then mixed with the clarified extracts and samples were incubated for 2 h at 4°C, followed by an additional 1-h incubation step at 4°C with 10 μl protein A/G magnetic beads (Thermo Fisher Scientific) pre-washed with TBST buffer. The beads were then washed five times with cold TBST buffer and once with ice-cold water. Bound proteins were directly eluted in SDS-PAGE sample buffer, resolved by SDS-PAGE, and immunoblotted with anti-Ub conjugated with horseradish peroxidase (Santa Cruz Biotechnology).

AUTHOR CONTRIBUTIONS

ZH designed the research; PY performed the experiments; PY and ZH analyzed the data and wrote the paper.

ACKNOWLEDGMENTS

We thank Drs. Richard S. Marshall and Richard D. Vierstra for providing the proteasome and autophagy antibodies. This work was supported by an NSF CAREER award (MCB-1750361 to ZH).

CONFLICT OF INTEREST

The authors have no conflicts of interest to report.

DATA AVAILABILITY STATEMENT

All relevant data can be found within the manuscript and its supporting materials.

SUPPORTING INFORMATION

Additional Supporting Information may be found in the online version of this article.

Figure S1. Confirmation of three proteasome and four autophagy T-DNA insertion mutants.

Figure S2. Phenotypic analyses of seed development in selected proteasome and autophagy mutants.

Figure S3. Disruption of both proteasome and autophagy members results in defective embryogenesis.

Figure S4. Correlation assay of relative expression between indicated proteasome and autophagy genes in siliques in four different developmental stages as described in Figure 1d.

Figure S5. A second experiment examining the development-dependent changes of protein ubiquitylation and autophagy flux in siliques using an immunoblot assay.

Figure S6. Proteasome members are equally downregulated during silique development between WT and *rpn10-1*.

Figure S7. Knock-down of *ATG7* in *atg7-2* does not perturb the transcript levels of six selected proteasome genes in 8-DAA siliques.

Figure S8. Stabilization of selected proteasome members in 3- and 8-DAA siliques by ConA.

Figure S9. Stabilization analysis of ATG5 and ATG5-ATG12 adducts in 7-day-old seedlings and 3- and 8-DAA siliques upon MG132 treatment.

Figure S10. MG132 treatment does not change the transcript levels of three selected autophagy genes.

Figure S11. Immunoprecipitation of ATG7 identifies its polyubiquitylation in 3-DAA siliques.

Figure S12. Comparison of vacuolar breakdown and stability of GFP-ATG8a in different tissues upon MG132 treatment.

Figure S13. Comparison of vacuolar breakdown and stability of GFP-ATG8a in different tissues upon ConA treatment.

Table S1. T-DNA insertion mutants used in this study.

Table S2. Normalized transcripts per million (TPM) values of selected UPS and autophagy genes in developing embryos.

Table S3. Primers used in this study.

Table S4. Antibodies used in this study.

REFERENCES

Anderson, L.E. (1954) Hoyer's solution as a rapid permanent mounting medium for bryophytes. *The Bryologist*, **57**, 242–244.

Beck, F., Unverdorben, P., Bohn, S., Schweitzer, A., Pfeifer, G., Sakata, E. *et al.* (2012) Near-atomic resolution structural model of the yeast 26S proteasome. *Proceedings of the National Academy of Sciences of the United States of America*, **109**, 14870–14875.

Book, A.J., Gladman, N.P., Lee, S.S., Scalf, M., Smith, L.M. & Vierstra, R.D. (2010) Affinity purification of the Arabidopsis 26S proteasome reveals a diverse array of plant proteolytic complexes. *The Journal of Biological Chemistry*, **285**, 25554–25569.

Book, A.J., Smalle, J., Lee, K.H., Yang, P., Walker, J.M., Casper, S. ***et al.*** (2009) The RPN5 subunit of the 26s proteasome is essential for gametogenesis, sporophyte development, and complex assembly in Arabidopsis. *Plant Cell*, **21**, 460–478.

Brukhin, V., Gheyselinck, J., Gagliardini, V., Genschik, P. & Grossniklaus, U. (2005) The RPN1 subunit of the 26S proteasome in Arabidopsis is essential for embryogenesis. *Plant Cell*, **17**, 2723–2737.

Chung, T., Phillips, A.R. & Vierstra, R.D. (2010) ATG8 lipidation and ATG8-mediated autophagy in Arabidopsis require ATG12 expressed from the differentially controlled *ATG12A* and *ATG12B* loci. *The Plant Journal*, **62**, 483–493.

Chung, T., Suttangkakul, A. & Vierstra, R.D. (2009) The ATG autophagic conjugation system in maize: ATG transcripts and abundance of the ATG8-lipid adduct are regulated by development and nutrient availability. *Plant Physiology*, **149**, 220–234.

Clavel, M. & Dagdas, Y. (2021) Proteasome and selective autophagy: brothers-in-arms for organelle quality control. *Current Opinion in Plant Biology*, **63**, 102106.

da Fonseca, P.C., He, J. & Morris, E.P. (2012) Molecular model of the human 26S proteasome. *Molecular Cell*, **46**, 54–66.

Di Berardino, J., Marmagne, A., Berger, A., Yoshimoto, K., Cueff, G., Chardon, F. ***et al.*** (2018) Autophagy controls resource allocation and protein storage accumulation in Arabidopsis seeds. *Journal of Experimental Botany*, **69**, 1403–1414.

Dikic, I. & Elazar, Z. (2018) Mechanism and medical implications of mammalian autophagy. *Nature Reviews. Molecular Cell Biology*, **19**, 349–364.

Ding, X., Zhang, X. & Otegui, M.S. (2018) Plant autophagy: new flavors on the menu. *Current Opinion in Plant Biology*, **46**, 113–121.

Doroodian, P. & Hua, Z. (2021) The ubiquitin switch in plant stress response. *Plants*, **10**, 246.

Dresselhaus, T. & Jurgens, G. (2021) Comparative embryogenesis in angiosperms: activation and patterning of embryonic cell lineages. *Annual Review of Plant Biology*, **72**, 641–676.

Dure, L.S., III. (1975) Seed formation. *Annual Review of Plant Physiology*, **26**, 259–278.

Finley, D. (2009) Recognition and processing of ubiquitin-protein conjugates by the proteasome. *Annual Review of Biochemistry*, **78**, 477–513.

Finley, D., Chen, X. & Walters, K.J. (2016) Gates, channels, and switches: elements of the proteasome machine. *Trends in Biochemical Sciences*, **41**, 77–93.

Finley, D. & Prado, M.A. (2020) The proteasome and its network: engineering for adaptability. *Cold Spring Harbor Perspectives in Biology*, **12**, a033985.

Gladman, N.P., Marshall, R.S., Lee, K.H. & Vierstra, R.D. (2016) The proteasome stress regulon is controlled by a pair of NAC transcription factors in Arabidopsis. *Plant Cell*, **28**, 1279–1296.

Glickman, M.H., Rubin, D.M., Coux, O., Wefes, I., Pfeifer, G., Cjeka, Z. ***et al.*** (1998) A subcomplex of the proteasome regulatory particle required for ubiquitin-conjugate degradation and related to the COP9-signalosome and eIF3. *Cell*, **94**, 615–623.

Groll, M., Ditzel, L., Lowe, J., Stock, D., Bochtler, M., Bartunik, H.D. ***et al.*** (1997) Structure of 20S proteasome from yeast at 2.4 a resolution. *Nature*, **386**, 463–471.

Guiboileau, A., Yoshimoto, K., Soulay, F., Bataille, M.P., Avice, J.C. & Masclaux-Daubresse, C. (2012) Autophagy machinery controls nitrogen remobilization at the whole-plant level under both limiting and ample nitrate conditions in Arabidopsis. *The New Phytologist*, **194**, 732–740.

Haller, M., Hock, A.K., Giampazolias, E., Oberst, A., Green, D.R., Debnath, J. ***et al.*** (2014) Ubiquitination and proteasomal degradation of ATG12 regulates its proapoptotic activity. *Autophagy*, **10**, 2269–2278.

Heinemeyer, W., Fischer, M., Krimmer, T., Stachon, U. & Wolf, D.H. (1997) The active sites of the eukaryotic 20 S proteasome and their involvement in subunit precursor processing. *The Journal of Biological Chemistry*, **272**, 25200–25209.

Hellmann, H. & Estelle, M. (2002) Plant development: regulation by protein degradation. *Science*, **297**, 793–797.

Hofmann, F., Schon, M.A. & Nodine, M.D. (2019) The embryonic transcriptome of *Arabidopsis thaliana*. *Plant Reproduction*, **32**, 77–91.

Holdsworth, M.J., Bentsink, L. & Soppe, W.J.J. (2008) Molecular networks regulating Arabidopsis seed maturation, after-ripening, dormancy and germination. *The New Phytologist*, **179**, 33–54.

Hua, Z., Doroodian, P. & Vu, W. (2018) Contrasting duplication patterns reflect functional diversities of ubiquitin and ubiquitin-like protein modifiers in plants. *The Plant Journal*, **95**, 296–311.

Hua, Z. & Vierstra, R.D. (2011) The cullin-RING ubiquitin-protein ligases. *Annual Review of Plant Biology*, **62**, 299–334.

Huang, H., Weiss, C.A. & Ma, H. (1994) Regulated expression of the Arabidopsis G protein α subunit gene *GPA1*. *International Journal of Plant Sciences*, **155**, 3–14.

Huang, X., Zheng, C., Liu, F., Yang, C., Zheng, P., Lu, X. ***et al.*** (2019) Genetic analyses of the Arabidopsis ATG1 kinase complex reveal both kinase-dependent and independent autophagic routes during fixed-carbon starvation. *Plant Cell*, **31**, 2973–2995.

Huss, M., Ingenhorst, G., Konig, S., Gassel, M., Drose, S., Zeeck, A. ***et al.*** (2002) Concanamycin a, the specific inhibitor of V-ATPases, binds to the V(o) subunit c. *The Journal of Biological Chemistry*, **277**, 40544–40548.

Ichimura, Y., Kirisako, T., Takao, T., Satomi, Y., Shimonishi, Y., Ishihara, N. ***et al.*** (2000) A ubiquitin-like system mediates protein lipidation. *Nature*, **408**, 488–492.

Jenik, P.D., Gillmor, C.S. & Lukowitz, W. (2007) Embryonic patterning in *Arabidopsis thaliana*. *Annual Review of Cell and Developmental Biology*, **23**, 207–236.

Jung, H., Lee, H.N., Marshall, R.S., Lomax, A.W., Yoon, M.J., Kim, J. ***et al.*** (2020) Arabidopsis cargo receptor NBR1 mediates selective autophagy of defective proteins. *Journal of Experimental Botany*, **71**, 73–89.

Kurepa, J., Wang, S., Li, Y., Zaitlin, D., Pierce, A.J. & Smalle, J.A. (2009) Loss of 26S proteasome function leads to increased cell size and decreased cell number in Arabidopsis shoot organs. *Plant Physiology*, **150**, 178–189.

Lander, G.C., Estrin, E., Matyskiela, M.E., Bashore, C., Nogales, E. & Martin, A. (2012) Complete subunit architecture of the proteasome regulatory particle. *Nature*, **482**, 186–191.

Lasker, K., Forster, F., Bohn, S., Walzthoeni, T., Villa, E., Unverdorben, P. ***et al.*** (2012) Molecular architecture of the 26S proteasome holocomplex determined by an integrative approach. *Proceedings of the National Academy of Sciences of the United States of America*, **109**, 1380–1387.

Lau, S., Slane, D., Herud, O., Kong, J. & Jurgens, G. (2012) Early embryogenesis in flowering plants: setting up the basic body pattern. *Annual Review of Plant Biology*, **63**, 483–506.

Le, B.H., Cheng, C., Bui, A.Q., Wagmaister, J.A., Henry, K.F., Pelletier, J. ***et al.*** (2010) Global analysis of gene activity during Arabidopsis seed development and identification of seed-specific transcription factors. *Proceedings of the National Academy of Sciences of the United States of America*, **107**, 8063–8070.

Leprince, O., Pellizzaro, A., Berriri, S. & Buitink, J. (2017) Late seed maturation: drying without dying. *Journal of Experimental Botany*, **68**, 827–841.

Li, F., Chung, T., Pennington, J.G., Federico, M.L., Kaeppler, H.F., Kaeppler, S.M. ***et al.*** (2015) Autophagic recycling plays a central role in maize nitrogen remobilization. *Plant Cell*, **27**, 1389–1408.

Li, F. & Vierstra, R.D. (2012) Autophagy: a multifaceted intracellular system for bulk and selective recycling. *Trends in Plant Science*, **17**, 526–537.
Marshall, R.S., Hua, Z., Mali, S., McLoughlin, F. & Vierstra, R.D. (2019) ATG8-binding UIM proteins define a new class of autophagy adaptors and receptors. *Cell*, **177**, 766–781.e24.
Marshall, R.S., Li, F., Gemperline, D.C., Book, A.J. & Vierstra, R.D. (2015) Autophagic degradation of the 26S proteasome is mediated by the dual ATG8/ubiquitin receptor RPN10 in Arabidopsis. *Molecular Cell*, **58**, 1053–1066.
Marshall, R.S. & Vierstra, R.D. (2018) Autophagy: the master of bulk and selective recycling. *Annual Review of Plant Biology*, **69**, 173–208.
Marshall, R.S. & Vierstra, R.D. (2019) Dynamic regulation of the 26S proteasome: from synthesis to degradation. *Frontiers in Molecular Biosciences*, **6**, 40.
Martinez-Fonts, K., Davis, C., Tomita, T., Elsasser, S., Nager, A.R., Shi, Y. *et al.* (2020) The proteasome 19S cap and its ubiquitin receptors provide a versatile recognition platform for substrates. *Nature Communications*, **11**, 477.
Masclaux-Daubresse, C. & Chardon, F. (2011) Exploring nitrogen remobilization for seed filling using natural variation in *Arabidopsis thaliana*. *Journal of Experimental Botany*, **62**, 2131–2142.
McLoughlin, F., Kim, M., Marshall, R.S., Vierstra, R.D. & Vierling, E. (2019) HSP101 interacts with the proteasome and promotes the clearance of ubiquitylated protein aggregates. *Plant Physiology*, **180**, 1829–1847.
Minina, E.A., Moschou, P.N. & Bozhkov, P.V. (2017) Limited and digestive proteolysis: crosstalk between evolutionary conserved pathways. *The New Phytologist*, **215**, 958–964.
Nair, U., Thumm, M., Klionsky, D.J. & Krick, R. (2011) GFP-Atg8 protease protection as a tool to monitor autophagosome biogenesis. *Autophagy*, **7**, 1546–1550.
Noda, N.N., Ohsumi, Y. & Inagaki, F. (2010) Atg8-family interacting motif crucial for selective autophagy. *FEBS Letters*, **584**, 1379–1385.
Palovaara, J., de Zeeuw, T. & Weijers, D. (2016) Tissue and organ initiation in the plant embryo: a first time for everything. *Annual Review of Cell and Developmental Biology*, **32**, 47–75.
Pohl, C. & Dikic, I. (2019) Cellular quality control by the ubiquitin-proteasome system and autophagy. *Science*, **366**, 818–822.
Qi, H., Li, J., Xia, F.N., Chen, J.Y., Lei, X., Han, M.Q. *et al.* (2020) Arabidopsis SINAT proteins control autophagy by mediating ubiquitylation and degradation of ATG13. *Plant Cell*, **32**, 263–284.
Sahu, I. & Glickman, M.H. (2021) Structural insights into substrate recognition and processing by the 20S proteasome. *Biomolecules*, **11**, 148.
Santos-Mendoza, M., Dubreucq, B., Baud, S., Parcy, F., Caboche, M. & Lepiniec, L. (2008) Deciphering gene regulatory networks that control seed development and maturation in Arabidopsis. *The Plant Journal*, **54**, 608–620.
Signorelli, S., Tarkowski, L.P., Van den Ende, W. & Bassham, D.C. (2019) Linking autophagy to abiotic and biotic stress responses. *Trends in Plant Science*, **24**, 413–430.
Smalle, J., Kurepa, J., Yang, P., Emborg, T.J., Babiychuk, E., Kushnir, S. *et al.* (2003) The pleiotropic role of the 26S proteasome subunit RPN10 in Arabidopsis growth and development supports a substrate-specific function in abscisic acid signaling. *Plant Cell*, **15**, 965–980.
Smalle, J. & Vierstra, R.D. (2004) The ubiquitin 26S proteasome proteolytic pathway. *Annual Review of Plant Biology*, **55**, 555–590.
Soto-Burgos, J., Zhuang, X., Jiang, L. & Bassham, D.C. (2018) Dynamics of autophagosome formation. *Plant Physiology*, **176**, 219–229.
Sreenivasulu, N. & Wobus, U. (2013) Seed-development programs: a systems biology-based comparison between dicots and monocots. *Annual Review of Plant Biology*, **64**, 189–217.
Svenning, S., Lamark, T., Krause, K. & Johansen, T. (2011) Plant NBR1 is a selective autophagy substrate and a functional hybrid of the mammalian autophagic adapters NBR1 and p62/SQSTM1. *Autophagy*, **7**, 993–1010.
Thompson, A.R., Doelling, J.H., Suttangkakul, A. & Vierstra, R.D. (2005) Autophagic nutrient recycling in Arabidopsis directed by the ATG8 and ATG12 conjugation pathways. *Plant Physiology*, **138**, 2097–2110.
Vierstra, R.D. (2009) The ubiquitin-26S proteasome system at the nexus of plant biology. *Nature Reviews. Molecular Cell Biology*, **10**, 385–397.
Wendrich, J.R. & Weijers, D. (2013) The Arabidopsis embryo as a miniature morphogenesis model. *The New Phytologist*, **199**, 14–25.
Xie, Z. & Klionsky, D.J. (2007) Autophagosome formation: core machinery and adaptations. *Nature Cell Biology*, **9**, 1102–1109.